Journal of Molecular Structure 981 (2010) 59–70

Contents lists available at ScienceDirect

Journal of Molecular Structure

journal homepage: www.elsevier.com/locate/molstruc

FT-IR, FT-Raman, NMR spectral analysis and theoretical NBO, HOMO–LUMO analysis of bis(4-amino-5-mercapto-1,2,4-triazol-3-yl)ethane by *ab initio* HF and DFT methods

S. Subashchandrabose [a], Akhil R. Krishnan [a], H. Saleem [a,*], V. Thanikachalam [b], G. Manikandan [b], Yusuf Erdogdu [c]

[a] Department of Physics, Annamalai University, Annamalai Nagar 608 002, India
[b] Department of Chemistry, Annamalai University, Annamalai Nagar 608 002, India
[c] Department of Physics, Faculty of Arts and Science, Ahi Evran University, Kirsehir, Turkey

ARTICLE INFO

Article history:
Received 2 June 2010
Received in revised form 15 July 2010
Accepted 15 July 2010
Available online 21 July 2010

Keywords:
FT-IR
FT-Raman
NBO analysis
HOMO–LUMO
NMR
BAMTE

ABSTRACT

A combined experimental and theoretical studies were conducted on the molecular structure and vibrational spectra of bis(4-amino-5-mercapto-1,2,4-triazol-3-yl) ethane (BAMTE). The FT-IR and FT-Raman spectra of BAMTE were recorded in the solid phase. The molecular geometry and vibrational frequencies of BAMTE in the ground state have been calculated by using the *ab initio* HF (Hartree–Fock) and density functional methods (B3LYP) invoking 6-311++G(d,p) basis set. The optimized geometric bond lengths and bond angles obtained by HF method shows best agreement with the experimental values. Comparison of the observed fundamental vibrational frequencies of BAMTE with calculated results by HF and density functional methods indicates that B3LYP is superior to the scaled Hartree–Fock approach for molecular vibrational problems. The difference between the observed and scaled wave number values of most of the fundamentals is very small. The thermodynamic functions and atomic charges of the title compound was also performed at HF/B3LYP/6-311++G(d,p) level of theories. A detailed interpretation of the FT-IR, FT-Raman, NMR spectra of BAMTE was also reported. The theoretical spectrograms for Infrared and Raman spectra of the title molecule have been constructed. Natural bond orbital analysis has been carried out to explain the charge transfer or delocalization of charge due to the intra-molecular interactions. Energy of the highest occupied molecular (HOMO) orbital and lowest unoccupied (LUMO) molecular orbital have been predicted.

1. Introduction

A number of 1,3,4-thiadiazoles showed antibacterial properties similar to those of well known sulphonamide drugs [1]. Thus, the thiadiazole nucleus which incorporates an N—C—S linkage exhibits a large number of biological activities [2]. The utilization of the 1,2,4-triazole moiety as a part of ligand system in metal complexes has gained considerable attention in recent years [3–7]. The application of triazole ligands lies in medical research – complex with Pt(II) [8] exhibit antitumor activity (human cancer) similar to *cisplatin*. Triazole derivatives are also used in the synthesis of antibiotics, fungicides, herbicides, plant growth hormone regulators [9], and potentially good corrosion inhibitors [10,11].

Dickinson et al. [12] reported 2-aryl-1-(1H-1,2,4-triazol-1-yl) butan-2-ol derivatives with high activity against *Aspergillus fumigatus*. Replacement of one triazole ring of fluconazole with 4-pyridinyl leads to an increase in activity against *Aspergillus* and introduction of an α-methyl group has a marked additional beneficial effect. Investigation of pyridinyl and pyrimidinyl analogues resulted in the identification of 30 (UK-109, 496, voriconazole) which has excellent potency against a broad range of fungal pathogens including fumigatus and *Candida krusei*.

The incidence of systemic fungal infections such as *Candidosis*, *Cryptococcosis* and *Aspergillosis* has been increasing recently due to an increase in the number of immunocompromised hosts. For the treatment of these infections, the new antifungal azoles have been developed for clinical use. Attention has been paid to triazole derivatives because of their generally broad antifungal spectrum and low toxicity [13,14]. The main objective of this paper is to find theoretical methods that would offer a higher certainty of finding molecular structure parameters and vibrational wavenumbers. In addition to this HOMO, LUMO, NBO analysis has been used to elucidate the information regarding charge transfer within the molecule.

* Corresponding author. Tel.: +91 9443879295.
E-mail address: saleem_h2001@yahoo.com (H. Saleem).

0022-2860/$ - see front matter © 2010 Elsevier B.V. All rights reserved.
doi:10.1016/j.molstruc.2010.07.025

2. Experimental details

The compound bis(5-mercapto-4-amino-1,2,4-triazol-3-yl)ethane (BAMTE) in the solid form was synthesized, it was used as such without further purification. The FT-Raman spectrum of BAMTE has been recorded using 1064 nm line of Nd: YAG laser as excitation wavelength in the region 50–3500 cm^{-1} on a thermo Electron Corporation model Nexus 670 spectrophotometer equipped with FT-Raman module accessory. The FT-IR spectrum of this compound was recorded in the range of 400–4000 cm^{-1} on Nexus 670 spectrophotometer using KBr pellet technique. The spectrum was recorded at room temperature, with scanning speed of 30 $cm^{-1}min^{-1}$ and the spectral resolution of 4.0 cm^{-1}. The spectral measurements were carried out at Central Electro Chemical Research Institute (CECRI), Karaikudi, Tamil Nadu.

The ^{1}H and ^{13}C NMR spectra were recorded on a Bruker AMX 400 MHz for ^{1}H and 100 MHz for ^{13}C NMR in DMSO-d_6 with TMS as an internal standard, at Indian Institute of Science, Bangalore, India. The experimental FT-IR, FT-Raman and ^{1}H and ^{13}C NMR spectra are shown in Figs. 1–3. To understanding of chosen techniques, combined experimental and theoretical spectra have been predicted and explained in Figs. 4 and 5.

2.1. Synthesis procedure of bis(4-amino-5-mercapto-1,2,4-triazol-3-yl) ethane

A mixture of succinic acid (0.01 mol) and thiocarbohydrazide (0.02 mol) was warmed carefully until melting occurred and then it was kept at 170 °C for 30 min. The reaction mixture was then cooled and mixed with water (50 ml). The precipitate was filtered off, washed with water and 95% ethanol and finally recrystallized from DMF.

2.2. ^{1}H and ^{13}C NMR analysis

^{1}H NMR (DMSO-d_6, ppm): δ = 13.49(s, 2H, 2NH) two NH protons of the amino group,

δ = 5.56(s, 4H, $2NH_2$), two NH_2 protons, 3.06(s, 4H, $2CH_2$) methylene protons of the two CH_2 groups. ^{13}C NMR (DMSO-d_6, ppm): δ = 150.67 (C=N), δ = 165.91 and 162.20 (C=S) end group of thione.

3. Computational details

The entire calculations were performed at *ab initio* HF and DFT levels on a Pentium IV/3.02 GHz personal computer using *Gaussian*

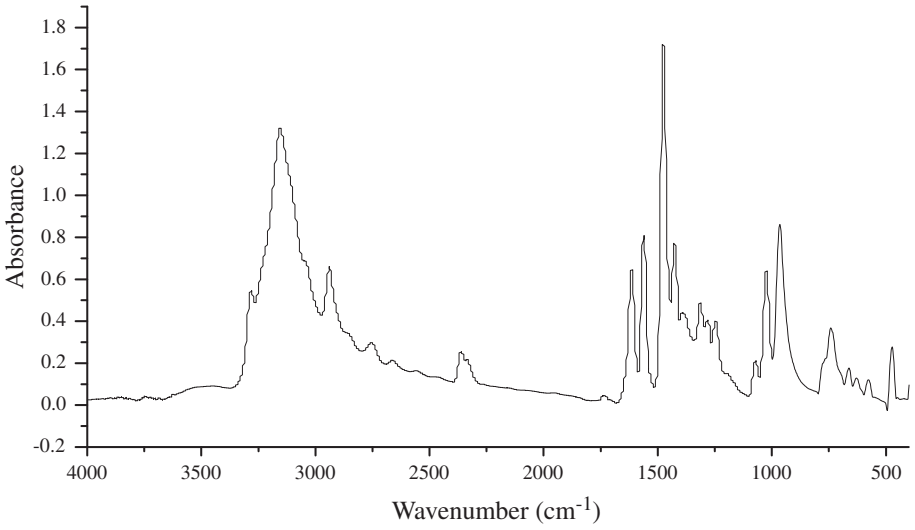

Fig. 1. Experimental FT-IR spectrum of BAMTE.

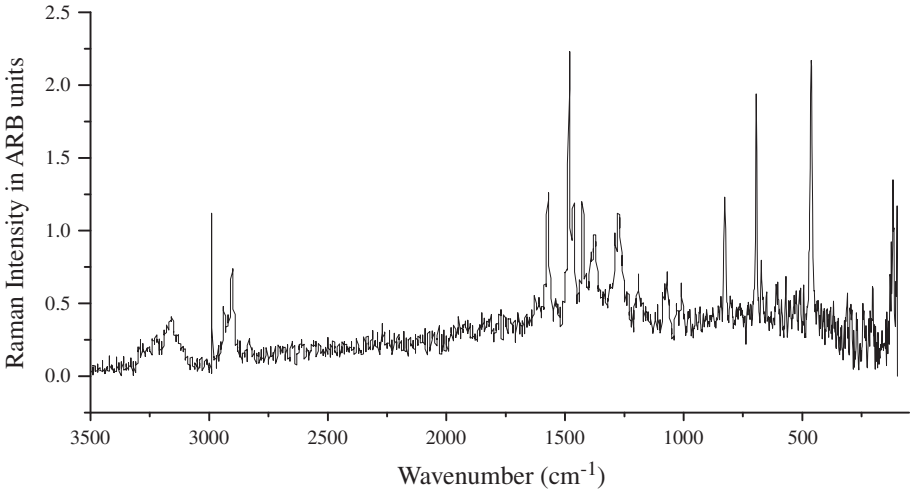

Fig. 2. Experimental FT-Raman spectrum of BAMTE.

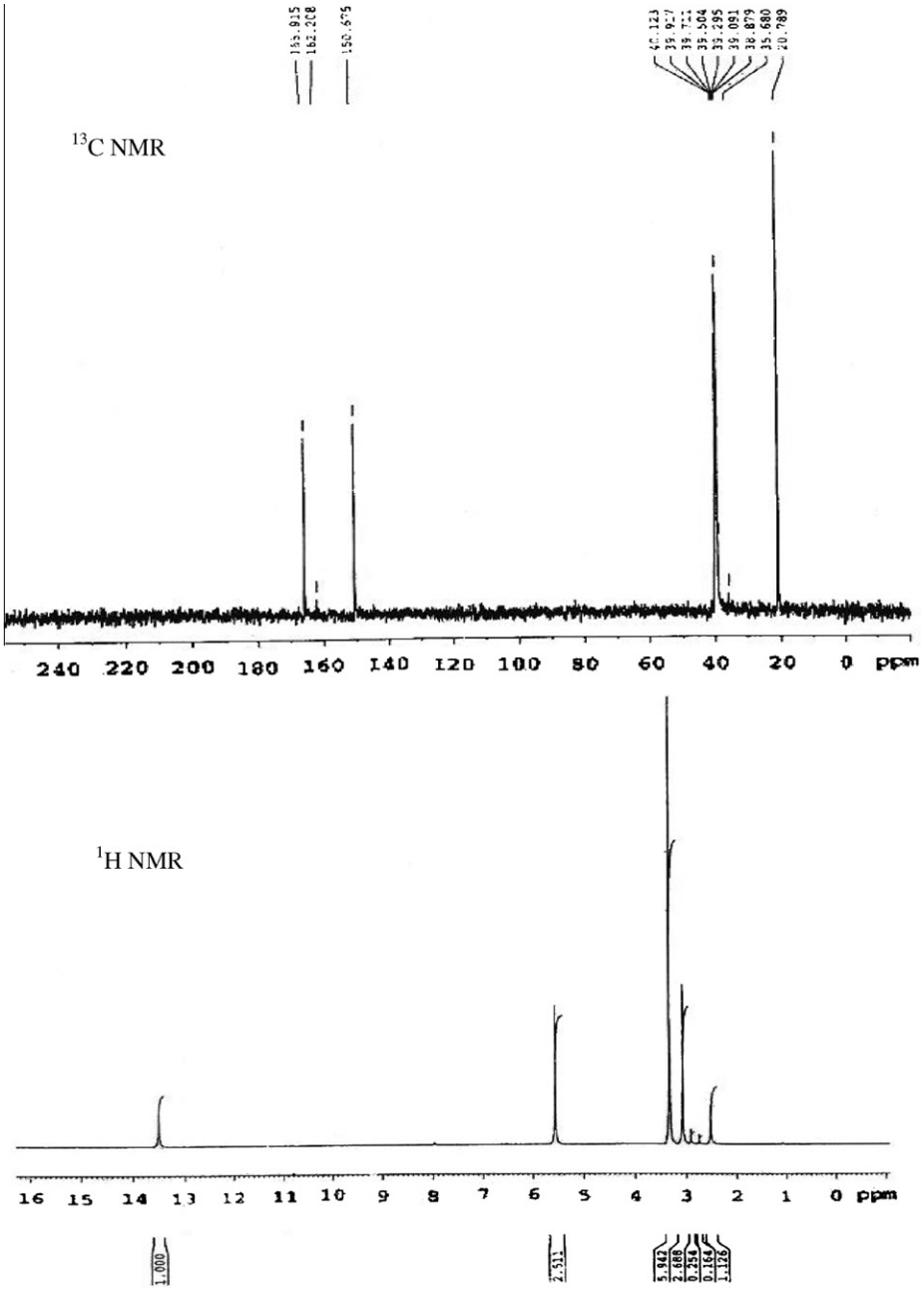

Fig. 3. ^{13}C and ^{1}H NMR spectra of BAMTE in DMSO-*d6*.

03 W [15] program package, invoking gradient geometry optimization [16]. Initial geometry generated from standard geometrical parameters was minimized without any constraint in the potential energy surface at *ab initio* HF level, adopting the standard 6-311++G(d,p) basis set. The optimized structural parameters were used in the vibrational frequency calculations at the *ab initio* HF and DFT levels to characterize all stationary points as minima. Then vibrationally averaged nuclear positions of BAMTE were used for harmonic vibrational frequency calculations resulting in IR and Raman frequencies together with intensities and Raman depolarization ratios. In this study, the DFT approach (B3LYP) has been utilized for the computation of molecular structure, vibrational frequencies and energies of optimized structures. Finally, the calculated normal mode vibrational frequencies provide thermodynamic properties also through the principle of statistical mechanics. By combining the results of the GAUSSVIEW program [17] with symmetry considerations, vibrational frequency assignments were made with a high degree of accuracy.

4. Results and discussion

4.1. Molecular geometry

The optimized structure parameters of BAMTE calculated by B3LYP *ab initio* (HF/6-311++G(d,p) basis set) are listed in Table 1. The atom numbering scheme also shown in Fig. 6 The present molecule consist of two triazole ring (namely 1,2,4-triazole), each azole ring attached with an amino group (namely 4-amino-1,2,4,-triazole). The two rings are joined with two methylene groups ($-CH_2-$ moiety) and some important atoms decorate the triazole molecule. In title molecule studied here, introduction of two substituent groups get changes in the bond distance. The distance

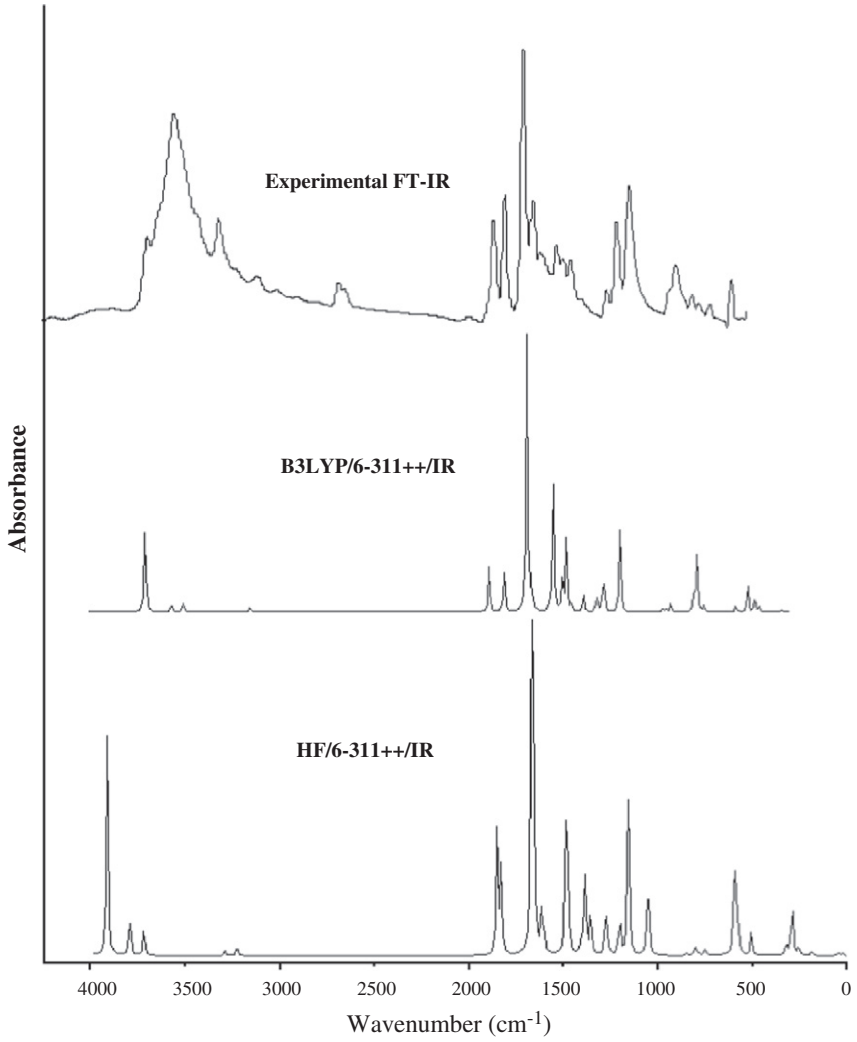

Fig. 4. Combined experimental and B3LYP/HF/6-311++G(d,p) IR spectrum of BAMTE.

between the atoms H9-N11 in the range 1.007 Å and 0.992 Å calculated by B3LYP/HF/6-311++G(d,p) level, respectively. While the bond distance between the carbon and sulphur atom (C1-S25) is in the range of 1.665 Å (DFT) and 1.672 Å (HF). Carbon and nitrogen atoms (C17–N18) are stands in the band distance of 1.301 Å range by B3LYP/6-311++G(d,p) method. This is in agreement with crystal structure of (1,2,4-triazole) ethane [18], in the range 1.298 Å. This may be due to the intra-molecular interaction with sulphur and hydrogen group. Distance between the N18-N23 falls in the range at 1.374 Å and 1.361 Å by B3LYP and HF methods, respectively.

Bond angle of nitrogen–carbon–nitrogen in the title molecule (N19–C1–N23) falls in the range of 101.464 Å by B3LYP method, 102.524 Å using HF 6-311++G(d,p). The bond angle of N19–C1–N23 is in agreement with [16]. The N18–C17–N19 bond angle falls in the range at 110.320 Å and 110.258 Å using DFT and *ab inito* HF respectively, which shows the closer agreement with literature value 110.25 Å [18]. The bond angle of N19–N20–H21 and N19–N20–H22 in the bis(4-amino-5-mercapto-1,2,4-triazol-3-yl) ethane falls in the range of 107.594 Å and 107.781 Å, respectively (DFT). Amino group (H21–N20–H22) bond angle lies at 106.121 Å and 107.271 Å by (DFT) and HF/6-311++G(d,p) methods respectively. The bond angle for methylene H3–C2–H4 and H6–C5–H7 groups is observed at 108.75 Å and 108.740 Å using DFT method. Based on the above comparison, there are some differences between the calculated and the literature value. The optimized structure parameters can well reproduce the literature values. The small difference between the computed data is due to calculation belongs to gaseous phase and experimental result belong to solid phase.

4.2. Vibrational assignments

The BAMTE possess C_s point group symmetry. The molecule has 26 atoms and 72 normal modes of fundamental vibrations which span the irreducible representations: (49A′ + 23A″). All the fundamental vibrations are active in both FT-IR and FT-Raman. The harmonic vibrational frequencies are calculated for BAMTE at B3LYP and HF level using the triple split valence basis set along with different and polarization function 6-311++G(d,p) are presented in Table 2. Comparison of frequencies calculated at HF and B3LYP with experimental values reveals the overestimation of the calculated vibrational modes due to neglect of harmonicity in real system. Inclusion of electron correlation in DFT values smaller in comparison with the HF frequencies data. The calculated frequencies are slightly higher than the observed values for the majority of the normal modes.

The major factor which is responsible for these discrepancies between the experimental and computed value is related to the fact that the experimental value is an anharmonic frequency while the calculated value is harmonic frequency. While anharmonicity

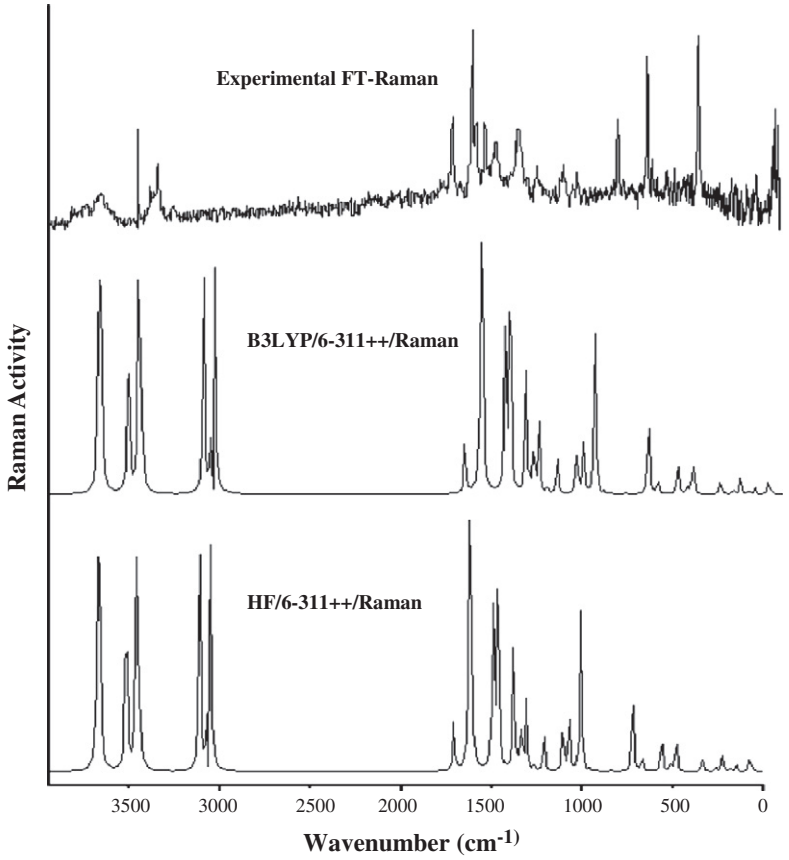

Fig. 5. Combined experimental and B3LYP/HF/6-311++G(d,p) FT-Raman spectrum of BAMTE.

is the main factor of the discrepancies in the case of vibrations related to the CH_2 or C═S bonds, for other vibrations most of the discrepancies come from the approximate nature of the used computational technique, and probably also from the lattice effects in the substance, studied as a solid.

In this study, there are two different scaling factors, one is 0.9668 for B3LYP and 0.9085 for HF methods [19] have been used and these are given as a foot note. The reduced mass and force constant along with the IR intensity and Raman activity are also included in Table 2. A comparison of the observed fundamental vibrational frequencies of the title compound with the calculated harmonic vibrational frequencies at B3LYP and HF levels using 6-311++G(d,p) basis set was performed. The frequency values computed at HF level contains known systematic error due to negligence of electron correlation. Therefore, a linearity between the experimental and calculated vibrational frequencies (i.e., for the whole spectral range considered), can be estimated by plotting the calculated versus experimental frequencies certain values obtained between the two methods, are strongly underestimated. As seen in Fig. 7 if these variations are omitted, *ab initio* HF and DFT/B3LYP calculations provide good linearity between the calculated and experimental frequencies (correlation coefficient of B3LYP & HF/6-31G(d,p) are 0.9990 and 0.9979, respectively). The small discrepancy observed between experimental and calculated frequencies may come from the formation of inter-molecular hydrogen bonding. Also we note that the experimental results belong to solid phase and the theoretical calculation belongs to gaseous phase.

4.2.1. CH_2 vibrations

The stretching modes of the CH_2 groups of dicorboxylic acids were recorded in the region 2950–2860 cm^{-1} [18]. The major coincidence of theoretical values with that of experimental values is found in the symmetric and asymmetric vibration of the methylene (–CH_2–) moiety. The CH_2 stretching vibration frequency assigned about 3100–2990 cm^{-1} in cyclohexane and other alkanes [20–22]. The CH_2 stretching frequency has computed in the range 2954–2966 cm^{-1} (symmetric), 3008–3025 cm^{-1} (asymmetric) by B3LYP method and 2921–2930 cm^{-1} (symmetric), 2972–2989 cm^{-1} (asymmetric) by HF method, mode Nos. (63–66). While the observed frequency is appeared in the range 2939 cm^{-1} (symmetric) in FT-IR at 2988 cm^{-1} and 3160 cm^{-1} (asymmetric) as medium strong bond in FT-Raman spectra.

The computed CH_2 asymmetric and symmetric vibrations mode show good agreement with literature as well as recorded spectrum. The CH_2 wagging vibration appears in the range at 1422, 1242 cm^{-1} in the noval compound 4-amino triazole adipic acid (4-atadip) [18]. Theoretically computed CH_2 wagging frequency has assigned in the range 1247 cm^{-1} and 1335 cm^{-1} by B3LYP/6-311++G(d,p) level, while the computed observations (HF method) are at 1277 cm^{-1} and 1394 cm^{-1}. The mode Nos. 46 and 52 (for both levels) are belongs to the above said vibration. For cyclohexane the CH_2 scissoring mode has been assigned to the medium intensity IR band at 1450 cm^{-1} [20,22]. The computed CH_2 scissoring modes are assigned in the range of 1416–1430 cm^{-1} and 1457–1471 cm^{-1} by DFT and HF, respectively (mode Nos. 54–56).

The frequency 965 cm^{-1} (FT-IR) is assigned to CH_2 twisting vibration in BAMTE molecule. The computed frequency range 970, 1195, 1295 cm^{-1} (DFT) and 999, 1232, 1341 cm^{-1} (HF) are assigned to CH_2 twisting mode and 35, 43, 49 are respective mode numbers. The experimental CH_2 twisting value shows good agreement with theoretical values. The CH_2 in-plane bending vibrations are appears at 1361, 1272, 1255 cm^{-1} in triazole [23]. The experi-

Table 1
Geometric bond length, bond angle and dihedral angle of BAMTE.

Parameters	B3LYP/6-311++G(d,p)	HF/6-311++G(d,p)	Experimental			
			a	c	d	b
Bond length (Å)						
C1—N19	1.390	1.360	1.353	1.380	1.356	1.343
C1—N23	1.356	1.327	1.330	1.299	1.309	1.309
C1—H24	2.105	2.067				
C1—S25	1.666	1.672				
C2—H3	1.093	1.084				
C2—H4	1.090	1.081				
C2—C5	1.549	1.539	1.401	1.467	1.504	
C2—C17	1.490	1.493				
C5—H6	1.090	1.081				
C5—H7	1.093	1.084				
C5—C10	1.490	1.493				
C8—N11	1.356	1.327				
C8—N13	1.390	1.360	1.344	1.378	1.347	1.325
C8—S26	1.666	1.672		1.674		
H9—N11	1.007	0.992		0.93		0.994
C10—N12	1.301	1.271				1.298
C10—N13	1.383	1.375				
N11—N12	1.374	1.361				
N13—N14	1.395	1.380		1.400		
N14—H15	1.019	1.002				0.994
N14—H16	1.019	1.002				
C17—N18	1.301	1.271				1.297
C17—N19	1.383	1.375				1.357
N18—N23	1.374	1.361				
N19—N20	1.395	1.380				1.392
N20—H21	1.019	1.002				
N20—H22	1.019	1.002				
N23—H24	1.007	0.992				
Bond angle (°)						
N19—C1—N23	101.46	102.52	101.80			
N19—C1—S25	127.68	127.67		127.97		
N23—C1—S25	130.86	129.81				
H3—C2—H4	108.75	108.83				
H3—C2—C5	109.13	109.61				
H3—C2—C17	109.31	109.08				
H4—C2—C5	109.94	110.35				
H4—C2—C17	107.10	106.81				
C5—C2—C17	112.53	112.07				
C2—C5—H6	109.95	110.35				
C2—C5—H7	109.13	109.61				
C2—C5—C10	112.54	112.08				
H6—C5—H7	108.74	108.83				
H6—C5—C10	107.10	106.80				
H7—C5—C10	109.31	109.08				
N11—C8—N13	101.46	102.52		102.80		
N11—C8—S26	130.86	129.81		129.23		
N13—C8—S26	127.68	127.67		127.97		
C5—C10—N12	125.22	125.38		125.90		
C5—C10—N13	124.45	124.35		123.84		
N12—C10—N13	110.32	110.26				
C8—N11—H9	125.24	125.37				
C8—N11—N12	114.41	113.76				
C9—N11—N12	120.34	120.87		122.07	123.80	
C10—N12—N11	104.55	104.85				
C8—N13—C10	109.26	108.61				
C8—N13—N14	125.89	126.59				
C10—N13—N14	124.84	124.79				
N13—N14—H15	107.78	108.51			106.00	
N13—N14—H16	107.59	108.39			110.00	
H15—N14—H16	106.12	107.27			113.00	
C2—C17—N18	125.22	125.39		125.90		
C2—C17—N19	124.45	124.35		123.84		
N18—C17—N19	110.32	110.26		110.25		
C17—N18—N23	104.54	104.85		104.24		
C1—N19—C17	109.26	108.61	104.3	108.16	106.20	101.0
C1—N19—N20	125.89	126.59		128.33	129.90	
C17—N19—N20	124.84	124.79		124.5		
N19—N20—H21	107.59	108.39				
N19—N20—H22	107.78	108.51				
H21—N20—H22	106.12	107.27				
C1—N23—N18	114.41	113.75		114.51		
C1—N23—H24	125.24	125.37				

Table 1 (*continued*)

Parameters	B3LYP/6-311++G(d,p)	HF/6-311++G(d,p)	Experimental			
			a	c	d	b
Dihedral angle (°)						
S25—C1—N19—C17	179.69	179.72				
S25—C1—N19—N20	0.78	1.08				
S25—C1—N23—N18	−179.67	−179.68				
S25—C1—N23—H24	−0.31	−0.16				
H3—C2—C5—H6	−60.82	−60.16				
H3—C2—C5—C10	58.47	58.72				
H4—C2—C5—C7	60.80	60.15				
H4—C2—C5—C10	−60.73	−61.12				
C17—C2—C5—H6	60.70	61.10				
C17—C2—C5—H7	−58.49	−58.74				
C17—C2—C5—C10	179.99	179.99				
H3—C2—C17—N18	−133.39	−133.29				
H3—C2—C17—N19	47.33	47.15				
H4—C2—C17—N18	−15.74	−15.81				
H4—C2—C17—N19	164.98	164.63				
C5—C2—C17—N18	105.19	105.15				
C5—C2—C17—N19	−74.09	−74.42				
C2—C5—C10—N12	−105.23	−105.17				
C2—C5—C10—N13	74.07	74.42				
H6—C5—C10—N12	15.70	15.79				
H6—C5—C10—N13	−165.00	−164.63				

Experimental values a, b, c, d are taken from.
[a] Ref. [16].
[b] Ref. [27].
[c] Ref. [32].
[d] Ref. [33].

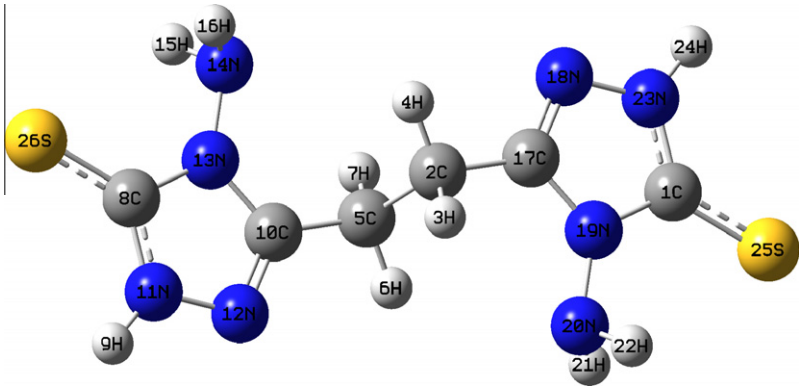

Fig. 6. Atom numbering scheme has been adopted in optimized structure of BAMTE.

mental observed CH_2 in-plane bending mode is observed at 1276 cm^{-1} (FT-Raman) and 1281 cm^{-1} (FT-IR). The computed CH_2 in-plane bending mode is observed at 1172 cm^{-1}, 1442–1568 cm^{-1} in DFT the same vibration exist in the HF method. The mode numbers 22, 27, 30, 31, are assigned to CH_2 rocking vibrations. While observed frequencies lie at 663, 742 cm^{-1} (FT-IR) and 673 cm^{-1} (FT-Raman) which show good agreement between observed and computed values.

4.2.2. NH_2 vibrations

The NH_2 group gives rise to the six internal modes of vibrations such as: the symmetric stretching (υ) the anti-symmetric stretching (υ') the symmetric deformation or the scissoring (δ), the rocking (ρ), the wagging (ω) and torsional mode (τ). The NH_2 group has two (N—H) stretching vibrations, one being asymmetric and other symmetric. The frequency of asymmetric vibration is higher than that of symmetric one. The absorption bands in the frequency range 3230–3381 cm^{-1} are attributed to the υNH_2 vibration of the amine group of the organic base [18].

In our title molecule BAMTE, the scaled NH_2 symmetric(υ) and asymmetric stretching modes are respectively in the range 3339–3398 cm^{-1} by B3LYP/6-311++G(d,p) level basis set and 3378–3445 cm^{-1} using HF/6-311++G(d,p) level (mode Nos. 67–70) is in agreement with experimental value of 3283 cm^{-1} NH_2 symmetric. The above assignment is in agreement with literature data [18]. The computed NH_2 scissoring is in the range 1651 (DFT) and 1681 cm^{-1} (HF) using 6-311++G(d,p) basis set (mode No. 61). For BAMTE the rocking mode predicted at 144–217 and 222 cm^{-1} (B3LYP) and 148–227 cm^{-1} and 260 (HF) mode nos: (6–10 and 12).

In our present study, the BAMTE NH_2 twisting frequency appears at 244 cm^{-1} in FT-Raman. The computed NH_2, twisting frequency assigned at 1312, 1313 cm^{-1} by DFT, which are in agreement with experimental values. While in the HF method, the NH_2 twisting values are in the range 1344, 1351 cm^{-1} (mode Nos. 50 and 51). The N—H out-of-plane bending vibrations are assigned at 467–505, 545, 654, 674 cm^{-1} (DFT: mode Nos. 19–21, 23, 26, 27) and 472–529, 547, 685 cm^{-1} (HF). The observed frequencies 663 cm^{-1} (FT-IR) 494, 502, 673 cm^{-1} (FT-Raman) is assigned

Table 2
Vibrational wave numbers obtained for BAMTE at B3LYP/HF /6-311++G(d,p) [harmonic frequency (cm^{-1}), IR, Raman Intensities (km/mol), Reduced masses (amu) and Force constants ($mdynA^{\circ -1}$)].

Mode No.	Experimental (cm^{-1})		Calculated frequencies at B3LYP/HF/6-311++G(d,p) (cm^{-1})						Red. Mass	Force Const.	Vibrational assignments
	FT-IR	FT-Raman	B3LYP	Intensity		HF	Intensity		6-311++G(d,p)		
				IR	Raman		IR	Raman			
1			17	0	0	19	0	0	7.45	0.00	Lattice vibration
2			31	0	0	34	0	0	7.13	0.00	Lattice vibration
3			39	0	0	40	1	0	8.29	0.01	Ring out-of-plane bending
4			61	0	1	76	0	1	4.09	0.01	γCH_2
5			75	0	2	78	0	2	8.42	0.03	Ring bending
6			144	0	1	148	0	1	4.74	0.06	$\rho NH_2 + \rho CH_2$
7			162	2	0	169	1	0	3.34	0.06	ρNH_2 in both ring
8			180	0	1	207	0	0	1.89	0.04	ρNH_2 in both ring
9			185	4	0	209	0	0	2.15	0.05	ρNH_2 in both ring
10		204 ms	217	0	0	227	0	3	1.72	0.05	ρNH_2 in both ring
11			220	0	3	233	2	0	4.36	0.13	$\rho CH_2 + \gamma N{-}H$
12			222	8	0	260	0	1	1.80	0.06	ρNH_2 in both ring
13			227	2	0	265	0	1	6.13	0.20	$\omega NH_2 + \rho CH_2$
14		244 ms	254	0	1	267	11	0	3.03	0.12	$\rho CH_2 + \omega NH_2$
15		295 w	287	2	0	294	2	0	3.15	0.16	$\rho CH_2 + \omega NH_2$
16		311 vw	325	0	3	338	0	3	11.64	0.78	$\gamma N{-}N{=}C$
17		369 vw	385	0	0	401	0	0	6.32	0.59	$\omega CH_2 + \gamma N{-}N + \gamma N{-}H$
18		462 vs	465	2	0	462	4	0	6.99	0.95	$\beta C{=}S$ + ring stretching
19	473 ms		467	0	6	472	0	5	5.36	0.74	$\gamma N{-}H + \rho CH_2 + \beta C{=}S$
20		494 vs	497	0	1	525	5	0	1.38	0.21	$\gamma N{-}H$
21		505 w	505	24	0	529	0	2	1.30	0.21	$\gamma N{-}H$
22			523	5	0	540	24	0	3.69	0.64	$\rho CH_2 + \omega NH_2$
23	577 w	569 w	545	0	7	547	0	2	4.52	0.85	$\gamma N{-}H + \gamma CH_2{-}CH_2 + \upsilon C{=}S$
24	628 w		646	0	2	669	0	2	8.08	2.12	$\gamma N{-}C{-}N + \gamma N{-}NH_2$
25			648	3	0	684	1	0	5.57	1.48	$\gamma N{-}C{-}H + \gamma N{-}C{-}N$
26			654	0	1	685	0	0	4.50	1.21	$\gamma N{-}H + \gamma C{-}H$
27	663 w	673 w	674	1	0	685	0	2	3.96	1.13	$\rho CH_2 + \gamma N{-}H + \gamma C{=}N$
28		694 vs	693	2	0	715	0	18	8.37	2.53	$\gamma C{=}N + \upsilon N{-}NH_2 + \beta C{-}N$
29			699	0	14	724	2	0	7.73	2.38	$\upsilon N{-}NH_2 + \beta C{-}H$
30	742 ms		729	1	0	735	1	0	3.58	1.20	$\rho CH_2 + \upsilon C{-}C$
31			753	0	0	769	0	0	1.76	0.63	ρCH_2
32		827 s	817	0	0	839	0	2	4.74	1.99	$\gamma CH_2{-}CH_2$
33			925	0	0	956	0	1	1.98	1.07	ωNH_2
34			929	29	0	958	19	0	2.18	1.19	ωNH_2
35	965 s		970	0	3	999	0	13	2.29	1.36	$tCH_2 + \beta N{-}H$
36			977	0	24	1003	0	3	4.68	2.81	$\upsilon CH_2{-}CH_2$
37		1009 ms	1019	16	0	1053	27	0	2.53	1.66	ωNH_2 + C—H bend + $\upsilon N{-}N$
38	1025 s		1037	0	11	1066	0	4	2.77	1.88	ωNH_2 + C—H bend
39			1057	7	0	1094	8	0	4.62	3.25	$\upsilon C{-}N + \beta N{-}H + \omega NH_2 + \upsilon N{-}N$
40	1072 w	1070 ms	1070	0	8	1111	0	6	4.78	3.45	$\upsilon N{-}N + \beta N{-}H + tCH_2 + \omega NH_2$
41			1133	6	0	1158	11	0	2.25	1.82	$tCH_2{+}\upsilon C{=}S$
42			1172	0	6	1204	0	11	4.69	4.06	$\upsilon C{-}N + \beta N{-}H + \beta C{-}H$
43		1189 ms	1195	4	0	1232	9	0	2.40	2.16	$tCH_2 + \upsilon C{=}S$
44			1223	0	1	1260	18	0	2.70	2.55	$\upsilon C{-}N + \upsilon C{=}S + \beta N{-}H$
45			1227	26	0	1260	0	12	2.17	2.06	$\upsilon C{-}N + \upsilon C{=}S + \beta N{-}H$
46	1246 ms		1247	10	0	1277	4	0	1.40	1.38	$\omega CH_2 + \beta N{-}H$
47			1265	0	12	1295	0	13	1.65	1.67	$tCH_2 + \beta N{-}H + \upsilon C{=}S$
48	1281 ms	1276 s	1292	0	9	1338	0	27	1.78	1.87	βCH_2 of $CH_3 + \beta N{-}H$ of NH_2
49			1295	44	0	1341	7	0	4.08	4.31	$\upsilon N{-}N + \beta N{-}N + \upsilon C{=}S + tCH_2$
50			1312	0	2	1344	0	12	1.16	1.26	tNH_2
51	1313 ms		1313	2	0	1351	31	0	1.18	1.28	tNH_2
52			1335	0	20	1394	0	15	1.65	1.85	ωCH_2
53			1416	6	0	1451	0	19	3.96	5.01	$\delta CH_2 + \delta NH_2 + \beta N{-}H + \upsilon N{-}N$
54	1392 ms		1416	0	43	1457	4	0	2.37	3.00	$\delta CH_2 + \beta N{-}H + \upsilon C{-}N$
55	1426 s	1425 s	1423	0	7	1469	8	0	1.43	1.83	$\delta CH_2 + \upsilon C{-}N$
56			1430	8	0	1471	0	16	1.19	1.53	δCH_2
57			1442	100	0	1513	100	0	2.64	3.46	$\upsilon N{-}C{=}S + \beta N{-}H + \beta C{-}H$
58			1443	0	30	1515	0	50	2.87	3.77	$\upsilon N{-}C{=}S + \beta N{-}H + \beta C{-}H$
59	1562 s		1565	0	92	1662	0	71	7.25	11.20	$\upsilon C{=}N + \beta N{-}H + \beta C{-}H$
60		1572 s	1568	15	0	1664	15	0	7.75	12.01	$\upsilon C{=}N + \beta N{-}H + \beta C{-}H + \delta CH_2$
61			1651	20	0	1681	20	0	1.10	1.89	δNH_2
62			1651	0	9	1682	0	13	1.10	1.90	δNH_2
63	2939 ms		2954	0	80	2921	0	100	1.06	5.84	υCH_2 symmetric stretch
64			2966	2	0	2930	2	0	1.06	5.89	υCH_2 symmetric stretch
65		2988 s	3008	0	35	2972	0	50	1.10	6.28	υCH_2 asymmetric stretch
66	3155 vs	3160 ms	3025	0	0	2989	1	0	1.10	6.36	υCH_2 asymmetric stretch
67	3283 ms		3339	4	5	3378	5	0	1.05	7.36	υNH_2 symmetric stretch
68			3339	0	89	3378	0	97	1.05	7.36	υNH_2 symmetric stretch
69			3398	2	21	3445	0	36	1.10	7.97	υNH_2 asymmetric stretch
70			3398	2	14	3445	6	1	1.10	7.97	υNH_2 asymmetric stretch

Table 2 (*continued*)

Mode No.	Experimental (cm^{-1})			Calculated frequencies at B3LYP/HF/6-311++G(d,p) (cm^{-1})					Red. Mass	Force Const.	Vibrational assignments
	FT-IR	FT-Raman	B3LYP	Intensity		HF	Intensity		6-311++G(d,p)		
				IR	Raman		IR	Raman			
71			3545	37	1	3553	33	16	1.08	8.58	υN—H stretching
72			3546	0	100	3554	6	84	1.08	8.58	υN—H stretching

ν – stretching, β – in-plane, γ – out-of-plane bending, ω – wagging, t – twisting, δ – scissoring, ρ – rocking, τ – torsion.
s – strong, m – medium, w – weak, v – very. scale factors: 0.9668 (B3LYP), 0.9085 (HF).

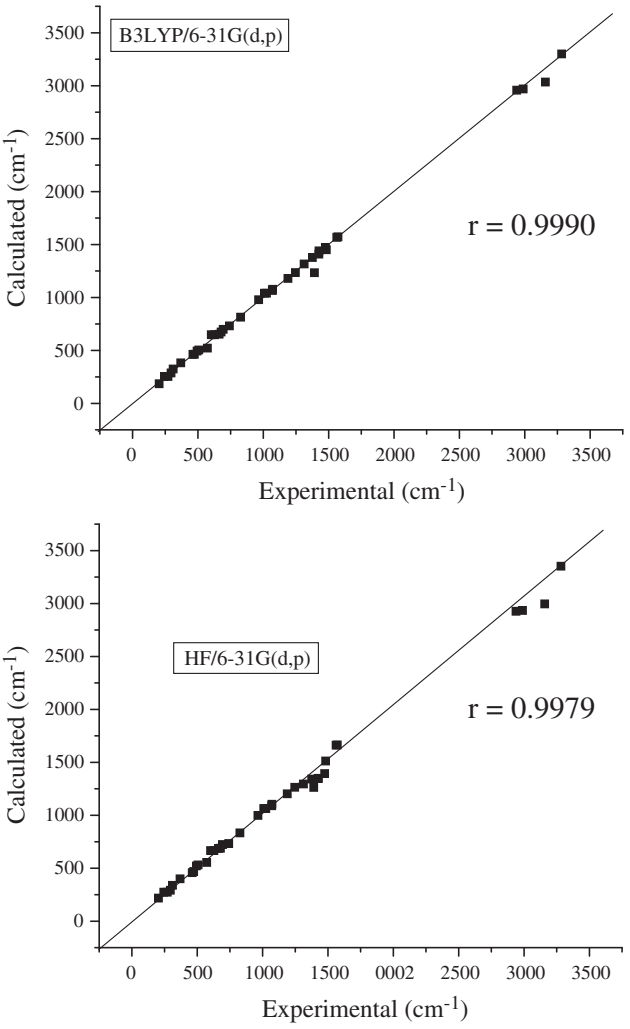

Fig. 7. Graphic correlation between the experimental and calculated frequencies obtained by DFT and HF/6-3G(d,p) of BAMTE.

to N—H out-of-plane bending vibration for the present molecule, which are in good agreement with the theoretical values.

4.2.3. C—N, C=N vibrations

The identification of C—N vibration is a very difficult task, since the mixing of several bands is possible in the region. Silverstein et al. [24] assigned C—N stretching absorption in the region 1382–1266 cm^{-1} for aromatic amines. In benzamide the band observed at 1368 cm^{-1} is assigned to be due to C—N stretching. In benzotrizole, the C—N stretching band is found to be present at 1382 and 1307 cm^{-1}. The frequencies 1411–1598 cm^{-1} in both FT-IR and FT-Raman spectra have been assigned to C—N, C=N stretching vibration, respectively [25]. In the present work, the strong bands observed in the range 1562, 1572 cm^{-1} (FT-IR, FT-Raman) have been assigned to C=N stretching vibration. The bands appears in the range 1392 cm^{-1} medium strong in FT-IR spectrum has been assigned to C—N stretching. Theoretically computed values of C=N vibration falls in the region 1565, 1568 cm^{-1} (DFT) and 1662, 1664 cm^{-1} (HF) in the both rings of the title molecule (mode Nos. 59 and 60). The both experimental and theoretical frequencies of C=N values show in agreement with the literature [25].

Experimentally observed C=N out-of-plane bending vibration falls in the range 694 cm^{-1} (very strong), in FT-Raman. The computed C=N out-of-plane bending vibration occurs at 674, 693 cm^{-1} and 685, 715 cm^{-1} (mode Nos. 27 and 28) using B3LYP and HF methods, respectively. The above observed experimental values of C=N out-of-plane bending vibration exactly coincide with theoretically computed values.

4.2.4. C=S vibrations

The C=S group is less polar than the C=O group and has a considerably weak band. Compound that contains a thiocarbonyl groups, which shows absorption in the region 1250–1020 cm^{-1} region Silverstein et al. [24]. In our present study, the C=S stretching frequency observed in the range 1189 cm^{-1} as a medium strong in FT-Raman spectrum and also C=S in-plane bending appear as a medium and strong band at 473 cm^{-1} and 462 cm^{-1} in FT-IR and FT-Raman, respectively. The scaled value of C=S stretching vibration occurs at 1133, 1195, 1223, 1227, 1265 and 1295 cm^{-1} (DFT) and 1158, 1232, 1260, 1295 and 1341 cm^{-1} (HF) using 6-311++G(d,p) basis set (mode Nos. 41, 43, 44, 45, 47, 49). The C=S in-plane bending vibrations obtained in the lower frequency range of 465 and 467 cm^{-1} in DFT method on the other hand in HF method 462, 472 cm^{-1} (mode Nos. 18 and 19) are assigned to same, which shows good agreement with the recorded experimental observations.

Table 3
Theoretically computed energies, zero-point vibrational energies (kcal/mol), rotational constants (GHz), entropies (cal mol^{-1} K^{-1}) and dipole moment (D) for BAMTE.

Parameters	B3LYP/6-31G(d,p)	B3LYP/6-311++G(d,p)	HF/63-1G(d,p)	HF/6-311++G(d,p).631G(d,p)
Total energy	−1469.01	−1469.24	−1463.60	−1463.80
Zero point energy	123.21	122.52	134.07	133.22
Rotational constants				
	1.496	1.507	1.544	1.547
	0.148	0.148	0.150	0.149
	0.137	0.137	0.139	0.139
Entropy				
Total	131.29	132.15	125.23	125.99
Translational	42.54	42.54	42.54	42.54
Rotational	33.62	33.62	33.57	33.57
Vibrational	55.12	55.98	49.11	49.88
Dipole moment	2.409	2.396	2.511	2.488

4.2.5. N—C—N bending vibrations

The FT-Raman bands at 688 and 623 cm^{-1} are assigned to C—N—C and N—C—C in-plane bending vibration respectively [25]. N—C—N out-of-plane bending vibration of BMATE has computed at 646, 648 cm^{-1} and 669 and 684 cm^{-1}, respectively (mode Nos. 24 and 25). N—N=C out-of-plane bending has observed in the range 311 cm^{-1} very weak band in FT-Raman, while the computed N—N=C out-of-plane bending has assigned at 325 cm^{-1} and 338 cm^{-1} using B3LYP and HF/6-311++G(d,p) level, respectively (mode No. 16), which is in agreement with experimentally observed frequencies.

4.3. Other molecular properties

Several calculated thermodynamic parameters are found by different basis sets and presented in Table 3. Scale factors have been recommended [26] for an accurate prediction in determining the zero-point vibration energy (ZPVE), and the entropy, $S_{vib}(T)$. The variations in the ZPVE's seem to be insignificant. The total energy and the change in the total entropy of BAMTE at room temperature at different methods are also presented.

4.4. NBO analysis

Natural bond orbital analysis gives the accurate possible natural Lewis structure picture of ø because all orbital are mathematically chosen to include the highest possible percentage of the electron density. Interaction between both filled and virtual orbital spaces information correctly explained by the NBO analysis, it could enhance the analysis of intra-inter-molecular interactions. The second order Fock matrix was carried out to evaluate donor (i) – acceptor (j) i.e. donor level bonds to acceptor level bonds interaction in the NBO analysis [27]. The result of interaction is a loss of occupancy from the concentration of electron NBO of the idealized Lewis structure into an empty non-Lewis orbital. For each donor (i) and acceptor (j), the stabilization energy $E(2)$ associates with the delocalization $i \rightarrow j$ is estimated as.

$$E^{(2)} = \Delta E_{ij} = q_i \frac{F(i,j)^2}{\varepsilon_j - \varepsilon_i}$$

where q_i is the donor orbital occupancy are ε_j and ε_i diagonal elements and $F(i,j)$ is the off diagonal NBO Fock matrix element. Natural bond orbital analysis provide an efficient method for studying intra and inter-molecular bonding and interaction among bonds, and also provides a convenient basis for investigating charge transfer or conjugative interaction in molecular systems. Some electron donor orbital, acceptor orbital and the interacting stabilization energy resulted from the second-order micro-disturbance theory are reported [28,29]. The larger $E(2)$ value the more intensive is the interaction between electron donors and acceptor i.e. the more donation tendency from electron donors to electron acceptors and the greater the extent of conjugation of the whole system [30]. Delocalization of electron density between occupied Lewis-type (bond or lone pair) NBO orbitals and formally unoccupied (antibond or Rydgberg) non-Lewis NBO orbital correspond to a stabilizing donor- acceptor interaction. NBO analysis has been performed on the BAMTE molecule at the DFT/B3LYP/6-311++G(d,p) level in order to elucidate, the intra-molecular rehybridization and delocalization of electron density within the molecule. Maximum energy transfer from lone pair S(25) to C1–N23 (65.29 kJ/mol), this investigation deeply mentioned the energy delocalization from the lone pair of the molecule to other part, which are listed in Table 4.

Table 4
Second order perturbation theory analysis of Fock matrix in NBO basis for BAMTE.

Donor (i)	ED/e	Acceptor (j)	ED/e	[a]$E(2)$ (kJ/mol)	[b]$E(j)-E(i)$ (a.u)	[c]$F(i,j)$ (a.u)
C2—C5	1.97	C2—H3	0.02	0.58	1.03	0.022
		C2—H4	0.01	0.52	1.03	0.021
		C2—C17	0.02	0.87	1.04	0.027
		C5—C10	0.02	1.02	1.05	0.029
		C10—N12	0.32	4.33	0.58	0.048
		C10—N13	0.05	0.95	1.01	0.028
C8—S26(1)	1.99	C8—S26	0.01	6.86	0.17	0.036
C8—S26(2)	1.98	C10—N13	0.05	2.79	1.02	0.048
		N11—N12	0.02	1.67	0.94	0.035
C17—N18	1.98	C1—S25	0.02	0.90	1.02	0.027
		C2—C5	0.02	0.58	1.17	0.023
		C2—C17	0.02	1.17	1.25	0.034
		N19—N20	0.02	3.90	1.08	0.058
		N23—H24	0.07	4.82	1.17	0.068
C17—N18	1.91	C1—N23	0.60	8.86	0.24	0.048
		C2—H3	0.02	2.90	0.74	0.042
		C2—H4	0.01	0.57	0.74	0.019
		C2—C5	0.02	0.78	0.67	0.021
LPN11	1.60	C8—S26	0.58	61.58	0.20	0.103
		C10—N12	0.02	25.66	0.25	0.073
LPN12	1.95	C8—N11	0.07	5.67	0.76	0.059
		C10—N13	0.05	4.69	0.82	0.055
		N13—N14	0.02	0.66	0.70	0.019
LPN13	1.58	C8—S26	0.58	62.67	0.21	0.107
		C10—N12	0.32	45.35	0.26	0.100
		N14—H15	0.01	4.66	0.72	0.058
		N14—H16	0.01	2.98	0.73	0.047
LPN14	1.96	C8—N13	0.08	9.79	0.73	0.076
		C10—N12	0.02	0.56	0.79	0.019
		C10—N13	0.05	1.25	0.76	0.028
LPN18	1.95	C1—N23	0.07	5.49	0.74	0.057
		C17—N19	0.05	4.62	0.83	0.055
		N19—N20	0.02	0.60	0.70	0.018
		N23—H24	0.07	2.86	0.79	0.043
LPN19	1.58	C1-N23	0.60	55.99	0.22	0.103
		C17—N18	0.33	46.08	0.26	0.101
		N20—H21	0.01	3.02	0.72	0.047
		N20—H22	0.01	4.74	0.71	0.058
LPN20	1.99	C1—N19	0.15	9.20	0.74	0.075
		C5—H6	0.01	1.59	0.81	0.032
		C5 —C10	0.02	1.74	0.81	0.034
		C17—N19	0.05	1.44	0.77	0.030
LPS25(1)	1.99	C1—N19	0.10	2.32	1.07	0.045
		C1—N23	0.07	3.19	1.01	0.051
LPS25(2)	1.84	C1—N19	0.10	10.89	0.56	0.071
		C1—N23	0.60	8.91	0.50	0.061
		N23—H24	0.07	6.56	0.55	0.055
LPS25(3)	1.67	C1—N23	0.60	65.29	0.11	0.081
LPS26(1)	1.99	C8—N11	0.07	2.99	1.03	0.050
		C8—N13	0.08	2.67	1.06	0.048
LPS26(2)	1.88	C8—N11	0.07	10.18	0.52	0.066
		C8—N13	0.08	10.93	0.55	0.070

[a] $E(2)$ means energy of hyperconjucative interactions (stabilization energy).
[b] Energy difference between donor and acceptor i and j NBO orbitals.
[c] $F(i,j)$ is the Fock matrix element between i and j NBO orbital.

4.5. HOMO–LUMO analysis

The highest occupied molecular orbital (HOMO) and lowest unoccupied molecular orbital (LUMO) are the main orbital take part in chemical stability [31]. The HOMO represents the ability to donate an electron and LUMO as an electron acceptor. The HOMO and LUMO energy calculated by B3LYP and HF/6-

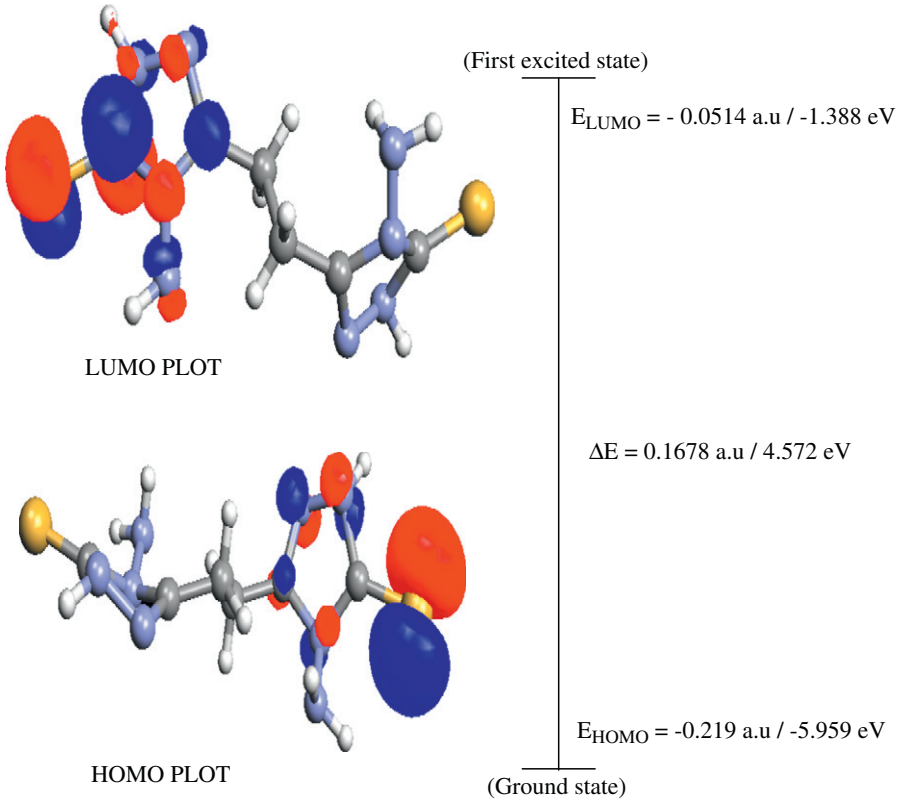

Fig. 8. The atomic orbital composition of the frontier molecular orbital for BAMTE.

Table 5
Some of the **c**alculated values of BAMTE in ground state at DFT and HF.

Methods	B3LYP/6-31G(d,p)	B3LYP/6-311++G(d,p)	HF/6-311++G(d,p)
Parameters			
HOMO (a.u/eV)	−0.207/−5.633	−0.219/−5.959	−0.311/−8.463
LUMO (a.u/eV)	−0.036/−0.980	−0.051/−1.388	0.026/0.708
Energy gap (Δ*E*) (a.u/eV)	0.171/4.653	0.168/4.572	0.285/7.755

311++G(d,p) method. The electronic transition absorption corresponds to the transition from the ground to the first excited state and is mainly described by an electron excitation from the highest occupied molecular orbital (HOMO) to the lowest unoccupied molecular orbital (LUMO). The HOMO is located over the C═S and C═N groups, the HOMO → LUMO transition implies an electron density transfer from triazole to C═S group. Moreover, the orbital significantly overlap in their position for BAMTE. The atomic compositions of the frontier molecular orbital are shown in Fig. 8. HOMO and LUMO energies calculated by B3LYP/HF in different basis sets are listed in Table 5. The calculated self-consistent field (SCF) energy of BAMTE is −107.9954 a.u (−2938.728 eV).

4.6. Atomic charges

Atomic charges of BAMTE molecule has been calculated using B3LYP and HF method at 6-31/6-311++G(d,p) are combined in Table 6. The calculated charges by B3LYP are relatively lesser than HF method. Atomic charge of C1in BAMTE is 0.87 and 1.05 using 6-311++G(d,p) level of DFT and HF, respectively. The maximum atomic charge is obtained for C1 and C8 when compare with other atoms in the bis(4-amino-5-mercapto-1,2,4-triazol-3-yl)ethane molecule. Illustration of atomic charges plotted for both 6-31G(d,p) and 6-311++G(d,p) level have been shown in Fig. 9.

Table 6
Atomic charges for optimized geometry of BAMTE.

Atom No.	B3LYP/6-31G(d,p)	HF/6-31G(d,p)	B3LYP/6-311++G(d,p)	HF/6-311++G(d,p)
C1	0.87	1.06	0.87	1.05
C2	0.11	0.13	0.10	0.13
H3	0.00	0.00	0.00	0.00
H4	0.00	0.00	0.00	0.00
C5	0.09	0.13	0.09	0.13
H6	0.00	0.00	0.00	0.00
H7	0.00	0.00	0.00	0.00
C8	0.86	1.06	0.87	1.05
H9	0.00	0.00	0.00	0.00
C10	0.44	0.53	0.43	0.54
N11	−0.16	−0.24	−0.17	−0.24
N12	−0.32	−0.39	−0.32	−0.40
N13	−0.40	−0.53	−0.43	−0.54
N14	0.16	0.20	0.17	0.21
H15	0.00	0.00	0.00	0.00
H16	0.00	0.00	0.00	0.00
C17	0.41	0.53	0.44	0.54
N18	−0.31	−0.39	−0.32	−0.40
N19	−0.41	−0.53	−0.43	−0.54
N20	0.16	0.20	0.17	0.21
H21	0.00	0.00	0.00	0.00
H22	0.00	0.00	0.00	0.00
N23	−0.17	−0.24	−0.17	−0.24
H24	0.00	0.00	0.00	0.00
S25	−0.64	−0.75	−0.65	−0.74
S26	−0.68	−0.75	−0.65	−0.74

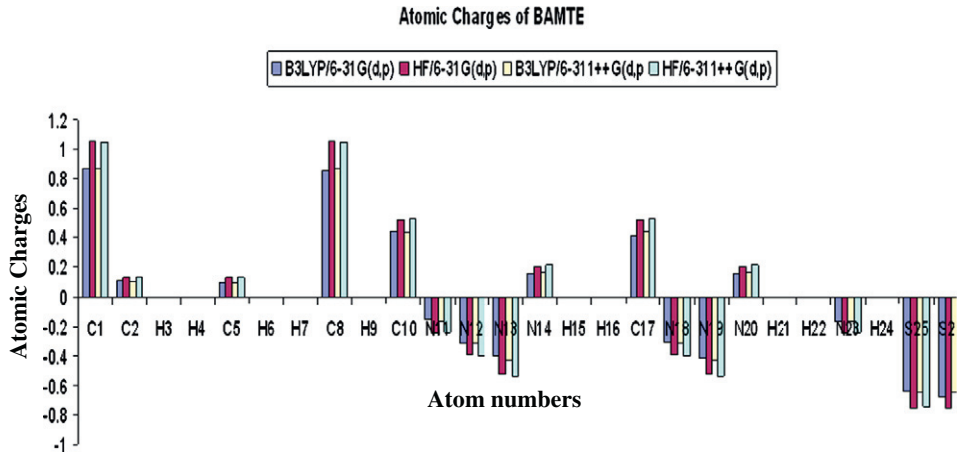

Fig. 9. Atomic charges of bis(4-amino-5-mercapto-1,2,4-triazol-3-yl)ethane.

5. Conclusion

In this present investigation molecular structure, vibrational frequencies, HOMO, LUMO, NBO and polarizability analysis of BAMTE have been studied using *ab initio* HF and DFT (B3LYP/6-311++G(d,p)) calculation. The FT-IR, FT-Raman and NMR (^{1}H and ^{13}C) spectral studies were carried out at first time. Any discrepancy noted between the observed and calculated frequencies may be due to the fact that the calculations have been actually done on a single molecule in the gaseous state contrary to the experimental values recorded in the presence of inter-molecular interactions. On the basis of the agreement between the calculated and observed results, assignments of fundamental vibrational modes of BAMTE were examined and some assignments are proposed. This study demonstrates that scaled DFT/B3LYP calculations are powerful approach for understanding the vibrational spectra of medium sized organic compound.

Acknowledgement

The authors are grateful to Dr. A.N. Kannappan, Professor and Head, Department of Physics, Annamalai University, for his constant help to complete this work successfully.

References

[1] J. Sandstrom, Adv. Heterocycl. Chem. 9 (1968) 165.
[2] A. Mohsen, M.E. Omar, A. Wafa, J. Heterocycl. Chem. 23 (1986) 1339.
[3] V.P. Sinditskii, V.I. Sokol, A.E. Fogel'zang, M.D. Dutov, V.V. Serushkin, A.P. Koshits, B.S. Svetlov, Zh. Neorg. Khim. 32 (1987) 1950.
[4] J.G. Haasnoot, Coord. Chem. Rev. 131 (2000) 200.
[5] M.H. Klingele, S. Brooker, Coord. Chem. Rev. 241 (2003) 119.
[6] U. Beckmann, S. Brooker, Coord. Chem. Rev. 245 (2003) 17.
[7] R.N. Muller, L.V. Elst, S. Laurent, Am. Chem. Soc. 125 (2003) 8405.
[8] S. Komeda, S. Bombard, S. Perrier, J. Reedijk, J. Kozelka, J. Inorg. Biochem. 96 (2003) 357.
[9] W. Li, Q. Wu, Y. Yu, M. Luo, L. Hu, Y. Gu, F. Niu, J. Hu, Spectrochim. Acta A60 (2004) 343.
[10] B. Mernari, H. Elattari, M. Traisnel, F. Bentiss, M. Langrenée, Corros. Sci. 40 (1998) 391.
[11] F. Bentiss, M. Langrenée, M. Traisnel, J.C. Hornez, Corros. Sci. 41 (1999) 789.
[12] R.P. Dickinson, A.S. Bell, C.A. Hitchcock, S. Narayanaswami, S. Ray, K. Richardson, P.F. Troke, Bioorg. Med. Chem. Lett. 6 (1996) 2031.
[13] D.J. Sheehan, C.A. Hitchcock, C.M. Sibley, Clin. Microbiol. Rev. 12 (1999) 40.
[14] R.S. Upadhayaya, N. Sinha, S. Jain, Bioorg. Med. Chem. 12 (2004) 2225.
[15] Gaussian 03 Program, Gaussian Inc., Walling ford CT, 2004.
[16] H.B. Schlegel, J. Comput. Chem. 3 (1982) 214.
[17] A. Frisch, A.B. Nielson, A.J. Holder, GAUSSVIEW User Manual, Gaussian Inc., Pittsburgh, PA, 2000.
[18] I. Matulkova, I. Nermec, K. Teubuer, P. Nemec, Z. Micka, J. Mol. Struct. 873 (2008) 46.
[19] A.P. Scott, L. Radom, J. Phys. Chem. 100 (1996) 16502.
[20] K.B. Wiberg, A. Shrake, Spectrochim. Acta A29 (1973) 583.
[21] L.J. Bellamy, The Infrared Spectra of Complex Molecule, Chapmann & Hall, London, 1975 (Chapters 2, 5, 12).
[22] R.G. Snyder, A. Shrake, Specrochim. Acta A29 (1965) 169.
[23] F. Billes, H. Endrédi, G. Keresztruy, J. Mol. Struct. 530 (2000) 183.
[24] M. Silverstein, G.C. Basselar, C. Morill, Spectrometric Identification of Organic Compounds, Wiley, NewYork, 1981.
[25] N. Sundaraganesan, K. Satheshkumar, C. Meganathan, B.D. Joshua, Spectrochim. Acta A65 (2006) 1186.
[26] M.A. Palafox, Int. J. Quantum Chem. 77 (2000) 661.
[27] M. Szafran, A. Komasa, E.B. Adamska, J. Mol. Struct. (THEOCHEM) 827 (2007) 101.
[28] C. James, A. Amal Raj, R. Rehunathan, I. Hubert Joe, V.S. Jayakumar, J. Raman Spectrosc. 379 (2006) 381.
[29] Jun-na Liu, Zhi-rang Chen, Shen-fang Yuan, J. Zhejiag Univ. Sci. 6B (2005) 584.
[30] S. Sebastian, N. Sundaragnesan, Spectrochim. Acta A75 (2010) 941.
[31] S. Gunasekaran, R.A. Balaji, S. Kumerasan, G. Anand, S. Srinivasan, Can. J. Anal. Sci. Spectrosc. 53 (2008) 149.
[32] A.L. Edwards, An Introduction to Linear Regression and Correlation, WH Freeman, San Francisco, 1976. p. 33.
[33] F. Guédira, M. Castella-Ventura, S. Zaydoun, A. Elhajji, A. Lautie, M. Saidi Idrissi, Spectrochim. Acta A73 (2010) 738.